Direct single-cell observation of a key *E. coli* cell cycle oscillator

Ilaria Iuliani[1,2,3], Gladys Mbemba[1], Marco Cosentino Lagomarsino[3,4,*] & Bianca Sclavi[2,*]

[1] *Université Paris-Saclay, ENS Paris-Saclay, CNRS, LBPA, 91190, Gif-sur-Yvette, France.*

[2] *LCQB, UMR 7238, CNRS, Sorbonne Université, 4 Place Jussieu 75005, Paris, France*

[3] *IFOM ETS – The AIRC Institute of Molecular Oncology, Milan, Italy, Via Adamello 16, 20139 Milan, Italy*

[4] *Dipartimento di Fisica, Università degli Studi di Milano, and I.N.F.N, via Celoria 16 20133 Milan, Italy*

**Equal contribution*

ABSTRACT

A long-standing hypothesis sees DNA replication control in *E. coli* as a central cell cycle oscillator at whose core is the DnaA protein. The consensus is that the activity of the DnaA protein, which is dependent on its nucleotide bound state, is an effector of initiation of DNA replication and a sensor of cell size. However, while several processes are known to regulate the change in DnaA activity, the oscillations in DnaA production and DnaA activity have never been observed at the single cell level, and their correlation with cell volume has yet to be established. Here, we measured the volume-specific production rate of a reporter protein under control of the *dnaA*P2 promoter in single cells. By a careful dissection of the effects of DnaA-ATP- and SeqA-dependent regulation of *dnaA*P2 promoter activity two distinct cell-cycle oscillators emerge. The first one, driven by both DnaA activity and SeqA repression, is strongly coupled to cell cycle and cell size, and its minima show the same "adder" behaviour as initiation events. The second, a reporter of DnaA activity, is still coupled with cell size but not to the time of cell division and its minima show a "sizer-like" behavior. These findings suggest that while DnaA activity and gene dosage perform volume sensing, SeqA repression primes the DnaA oscillator to follow extrinsic cues from cell cycle progression.

The DnaA protein is a key factor for the initiation of DNA replication and an essential protein for most known bacteria [1]. In *E. coli*, when it is in its ATP-bound form, DnaA binds to a set of specific sites at the origin of DNA replication leading to the formation of an oligomeric structure and the subsequent melting of an AT-rich region required for the assembly of the DNA replication forks [2–4]. At faster growth rates, initiation takes place at multiple copies of the origin to begin the synthesis of the genomes that terminates in daughter or granddaughter cells. The regulation of the timing and synchrony of initiation of DNA replication depends on the level of DnaA "activity", i.e. the amount of DnaA-ATP that is available to bind to its specific sites on the chromosome [2, 5–9].

While the classic idea of a "constant initiation mass per origin" is seriously challenged by recent data, there is some consensus that within a given condition and at the level of population averages, initiation of DNA replication is coupled to cell size and number of origins and that DnaA activity contributes to the setting of the initiation mass [7, 8, 10–15]. Furthermore, it is now a widely accepted idea that in single cells the added volume per origin between consecutive initiations may be constant and likely set by the contribution of the DnaA-dependent regulatory circuit [15–21]. However, a direct link is still missing between possible oscillations in DnaA activity and a constant inter-initiation added volume. Additionally, the debate is still heated regarding the additional question of whether and to what extent replication initiation sets the division time in single cells [15, 17–22]. This could occur because once initiation has taken place, the time required for genome replication and the subsequent time needed for cell division to be completed, the C and D periods respectively, tend to be constant at a given growth condition.

In *E. coli*, the DnaA-dependent regulatory circuit is made of different positive and negative components [6, 23]. Several factors contribute to the decrease in DnaA activity after initiation has taken place. Firstly, the expression of the *dnaA* gene is prevented for a fraction of the cell cycle by the SeqA protein binding to hemi-methylated GATC sites at the promoter after its replication[24–26]. Secondly, inhibition of transcription initiation by the oligomerisation of DnaA-ATP itself sets an upper limit to the cellular amount of DnaA-ATP [27–29]. Both of these processes inhibiting DnaA protein expression are related to initiation and fork progression. DnaA-ATP levels are expected to be the highest at the time of initiation and since the *dnaA* gene is close to the origin, SeqA causes a transient repression of the promoter right after each initiation. Thirdly, after initiation has taken place the hydrolysis of the ATP bound to DnaA is induced during ongoing DNA

replication via an interaction with the Hda protein mediated by the β-clamp in a process called RIDA (Regulatory Inactivation of DnaA) [30]. Finally, the binding of DnaA-ATP to the *datA* site also contributes to the conversion of DnaA-ATP to DnaA-ADP [31]. On the other hand, the increase in DnaA-ATP required for the initiation of a new DNA replication cycle depends in part on the timely accumulation of newly expressed protein [6, 25, 32] and the binding of DnaA to the DARS1 and DARS2 sites contributes to a further change in the DnaA-ATP to DnaA-ADP ratio by favoring the exchange of the DnaA-bound nucleotide [6, 33–35]. A recent study has shown that in the absence of RIDA, datA and DARS-dependent regulation, the intrinsic ATP hydrolysis activity of DnaA suffices to maintain a near-wild type replication cycle[36].

Given the complexity of this regulatory circuit, one of the major challenges in the field has been to find a way to measure the possible oscillations in DnaA activity in real time with little or no perturbation, at the level of the single cell. Here, we rely on a chromosomal promoter-reporter system based on the *dnaA* promoter itself as a reporter of the relative contributions of DnaA-ATP and SeqA on the expression of DnaA and to measure their relationship with cell size and cell division.

The DnaA promoter as a reporter of the changes in DnaA-ATP activity and SeqA *in vivo*

Since DnaA in the cell exists under two forms, ATP and and ADP bound, only the former being the one that can initiate DNA replication, we looked for a reporter of DnaA-ATP activity to study the regulation of DNA replication in *E. coli* in real time *in vivo*. We have chosen to use the role of DnaA as a transcription factor [39, 40] to report on the changes in DnaA activity. One of the best characterized targets of transcription regulation by DnaA is its own promoter. We have constructed a reporter cassette where the fast-folding *mut2-gfp* gene is under control of the *dnaA*P2 promoter sequence (dnaAP2, from -136 to +48 relative to the transcription start site). This GFP protein is highly soluble and stable [41]. This construct includes a Kanamycin resistance cassette expressed divergently upstream from the *dnaA* promoter.

Regulation of expression of the *dnaA* gene depends on a promoter region that includes two promoters, P1 and P2 [42]. P2 is found downstream of P1 and includes a GC-rich discriminator region overlapping with the transcription start site, making transcription initiation negatively regulated by ppGpp [43]. P2 is the stronger promoter in exponential phase and is thought to pro-

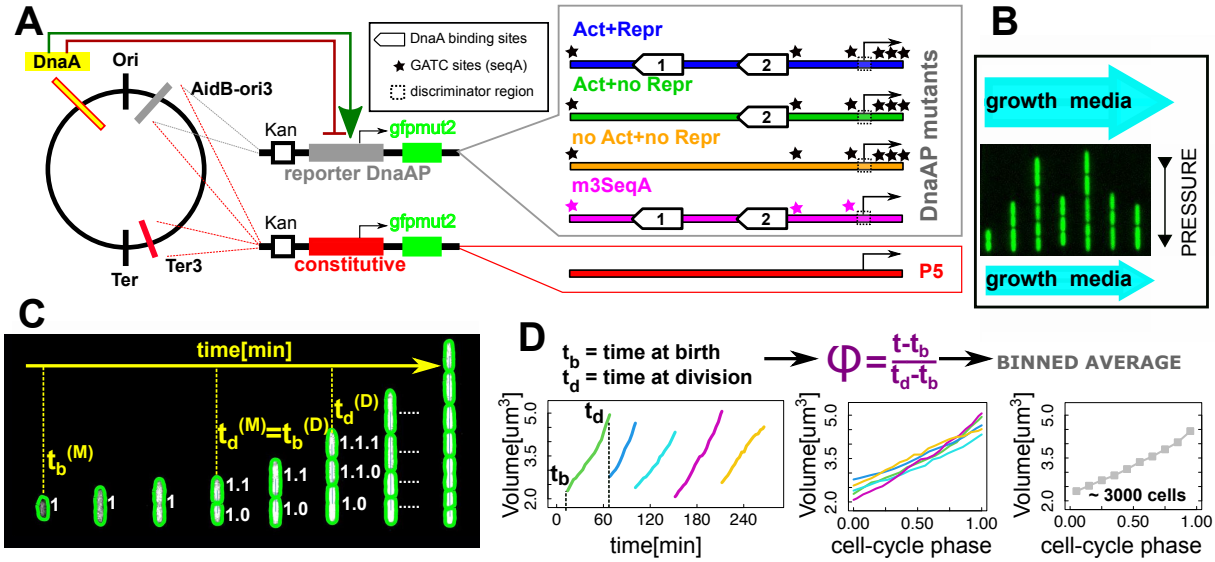

Figure 1: **Robust and long-term single cell tracking in fast growth conditions. (A)** We inserted a reporter construct of the *mut2gfp* gene at a specific site downstream of the *aidB* gene in the Ori macrodomain [37]. The reporter includes the native *dnaA*P2 promoter region and a Kanamycin resistance cassette upstream of the promoter. Different promoter mutants with different levels of regulation by DnaA and SeqA were considered. As a reference for baseline gene expression we used a constitutive promoter (see Methods). **(B)** The experimental device is a two-ended "mother machine" microfluidic channel where growth media flows constantly at the top and bottom of tapered-end micro-channels, ensuring a constant environment [38]. The picture shows a field of view with 7 micro-channels. Differences in flow rates between the two large channels generate a pressure that keeps the bacteria (which can only escape from the larger top end) inside the channels. **(C)** Segmentation/tracking algorithms follow the changes in cell size and fluorescence over time and across generations. The image shows snapshots of the same channel at subsequent times, and $t_{b,d}$ represent the times of birth/division of mother/daughter (M,D) in a lineage. **(D)** To examine the effects of cell cycle progression, we aligned growth and gene expression data with respect to cell cycle phase (fraction of the cell cycle), defined as cell cycle time normalized by the cell's division time.

vide the main growth-dependent regulation of DnaA expression, while P1 provides a basal level of constitutive expression, similarly to what is found at ribosomal promoter regions [29, 43, 44].

Expression from P2 is negatively regulated by a high concentration of DnaA-ATP, and positively regulated by DnaA when its concentration decreases [28, 29, 45], making it a potent sensor of DnaA-ATP levels. Specifically, two high-affinity sites for DnaA are found upstream of the dnaAP2 promoter, Box1 and Box2. The binding of DnaA-ATP to these two high-affinity sites activates transcription when DnaA-ATP activity is low. As DnaA-ATP concentration increases, the DnaA bound to Box1 and 2 becomes the scaffold for the formation of an oligomeric structure that represses transcription by occluding the RNA polymerase binding site [28, 29, 45]. Specific

mutations in Box1 and Box2 disrupt the DnaA-binding consensus sequence. These mutants decrease the binding affinity for DnaA and thus result in promoters that are only positively regulated (Box1 mutation) or neither positively nor negatively regulated by DnaA-ATP (Box1-Box2 mutation) [29]. Finally, transcription initiation is inhibited by SeqA binding to five GATC sites, two overlapping with the -10 and -35 sequences of P2 and three closely spaced sites found downstream of the transcription start site. An additional set of mutations ("m3SeqA", Fig. 1A) change the sequence of these three GATC sites. A previous study has shown that the set of these three mutations does not affect synchrony of initiation of DNA replication but causes a decrease in growth rate and DNA content in rich media[46]. The two GATC sites overlapping with the -10 and -35 sequence were left intact in order not to affect the binding of RNA polymerase, but a previous study has shown that they have little effect on repression by SeqA and DNA replication parameters[47]. As a further reference, we considered the expression of the same reporter fluorescent protein under control of a constitutive promoter used in a previous study [48]. This phage-derived constitutive promoter, "P5" in Fig. 1A, has consensus -10 and -35 sequences and lacks regulation by specific transcription factors, therefore its GFP production rate can be considered to be largely representative of the change in gene copy number with the passage of the DNA replication fork. To verify that its expression depends on when the gene copy number changes as a function of the cell cycle we have inserted the P5-GFP construct at the same origin-proximal locus as the *dnaA*P2-GFP construct (Ori3) as well as at the terminus-proximal locus (Ter3) downstream of the *uspE* gene (chromosome coordinate 1395706 bp).

The effect of the promoter mutations on GFP expression from the chromosomal insertion site have been measured by a plate reader assay and are consistent with the previously published results obtained on a plasmid [29] (Supplementary Figure S1). Mutation of Box1 increases expression relative to the wild type sequence, while mutation of both Box1 and 2 decreases expression back to wild type levels. What is important for this study is that (i) the original promoter ("Act+Repr" in Fig. 1A) senses both DnaA-ATP levels and the transit of the replication forks via the negative effect of SeqA binding (ii) the promoter stripped of both DnaA binding sites ("noAct+noRepr" in Fig. 1A) only senses the binding of SeqA, and (iii) the m3SeqA variant without the three GATC sites is only regulated by DnaA-ATP levels. In order to obtain an effect of SeqA on our reporter as similar as possible to the endogenous promoter, we have inserted the *dnaA*P2 promoter reporter cassette in the genome within the Ori macrodomain, at the "Ori3" locus downstream of the *aidB* gene (4413507 bp) [37] that was used in a previous study [48]. This site is at 21 percent of the

right replicore, the replication fork should pass through about 8 minutes after initiation of DNA replication.

To achieve single-cell resolution and capture the dynamic changes in cell growth, cell division and gene expression as a function of the cell cycle as well as across several generations, we used an integrated microfluidics and time-lapse microscopy approach [38]. In this device, an air pressure-controlled flow system provides a constant environment where cells can grow steadily for several days as the growth medium flows continuously at a constant rate (Fig. 1B and Supplementary Fig. S2). We mainly studied cells in a fast growth condition (M9 minimal medium with glucose and casamino acids at 30°C, where the cells have a mean doubling time of 45 minutes and initiate DNA replication at 2 origins). We also collected data at a slower growth condition (M9 minimal medium with glucose at 30°C, mean doubling time 75 minutes). Thousands of single cells were segmented and tracked from movies with frames obtained every 3 minutes to examine cell cycle dependent changes in fluorescent protein expression and cell size in lineages comprising up to 15 generations, as described in [48] (Fig. 1C). Supplementary Table S1 provides a complete list of measured parameters and computed variables. Each experiment yielded 2-8000 full cell cycles with a good reproducibility (Supplementary Fig. S3).

In absence of transcription regulation, GFP production rate increases with gene copy number and cell volume

To establish a solid reference for monitoring the cell cycle dependence of gene expression from the *dnaA*P2 promoter, our first goal was to characterize the "null" relationships between cell cycle progression and gene expression, i.e., the cell cycle variability of an unregulated promoter. To estimate the promoter activity in single cells, we defined a GFP production rate as the discrete time-derivative of fluorescence dF/dt from the time series of total fluorescence $F(t)$. Protein production rate can vary along the cell cycle because the replication of a gene at a specific moment in time doubles the probability that it will be expressed. Since gene replication occurs at a time in the cell cycle that depends on the gene's distance from the origin of DNA replication, the cell cycle dependence of its expression rate will depend on the gene's location along the genome. The copy number of a gene, g, changes during the cell cycle, and can be estimated quantitatively by a standard model [49], which also takes into account the case of overlapping DNA replication rounds, where replication forks from different initiation events are active in the same cell (see Methods).

Additionally, a protein's production rate has been observed to be proportional to cell size [50], probably in connection with the fact that cell size tends to be proportional to ribosome amounts. In our data, cell volume was computed considering a cell as a cylinder with two hemispherical caps where the radius was estimated from the segmented projected area (see Methods).

Supplementary Fig. S4A reports scatter plots of GFP production rate versus volume for origin- and terminus-proximal P5 constructs. These single-cell data show an average linear proportionality between the GFP production rate and cell volume, leading to an increase along the cell cycle. As expected from the estimation of average gene copy number, the same unregulated promoter shows an increased production rate when it is placed close to the replication origin compared to when it is found near the terminus. Normalizing the data by the estimated mean gene copy number (Eq. 3) removes most of this offset (Supplementary Fig. S4B), but the volume dependency remains.

In order to quantify the change in gene expression due to the increase in gene copy number as a function of cell cycle progression, we averaged the same data conditioning by cell cycle phase [51], defined as cell cycle time rescaled by the time between two consecutive divisions, i.e., t/τ (Supplementary Fig. S4AB). This procedure makes it possible to average together cells with all doubling times (3000-8000 cells in our case), hence increasing the statistical power. We found that the GFP production rate from the constitutive promoter is biphasic, which appears more clearly when the promoter is inserted close to the replication origin (Supplementary Fig. S4B). The beginning of the second phase correlates with the expected value of the cell cycle phase at which the gene is copied by DNA replication, supporting an effect of gene dosage. Rescaling the GFP production rate by cell volume and mean gene copy number highlights mild oscillations that are presumably due to cell cycle dependent gene dosage (Supplementary Fig. S4C). In particular, both the ori-proximal and the ter-proximal reporters increase their production after they are replicated. These small changes can be observed thanks to the large number of cell cycles analysed in our data.

In summary, GFP production from an unregulated promoter involves "null" cell cycle dependent trends due to volume and gene dosage, which in a regulated promoter have to be disentangled from any regulatory signal.

Transcription regulation by DnaA-ATP and SeqA causes strong oscillations in volume-specific GFP production rate

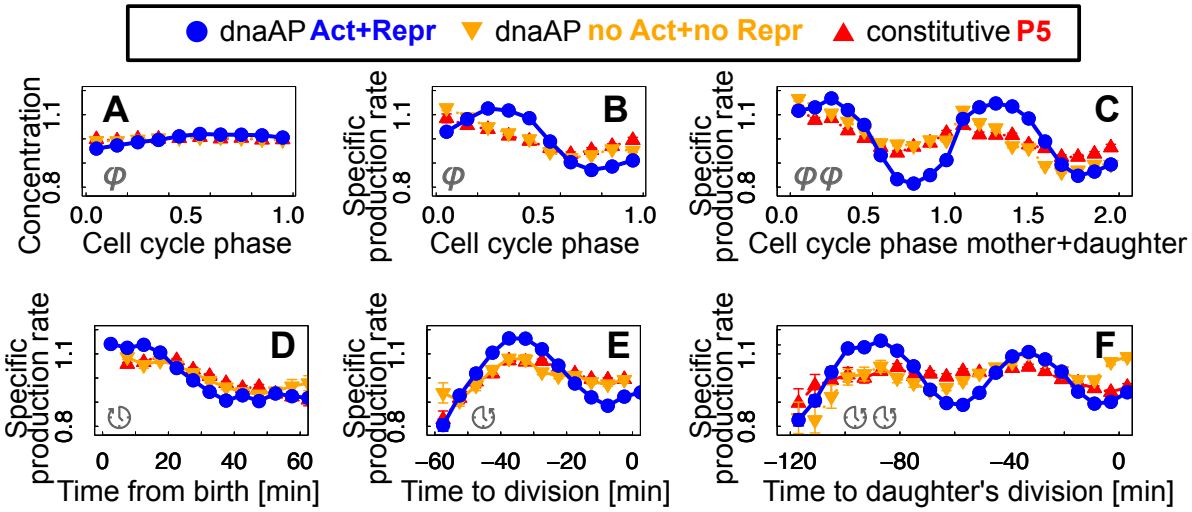

Figure 2: **Regulation of the *dnaA*P2 promoter by DnaA-ATP causes an oscillation in GFP production rate beyond the effect of gene dosage.** **(A)** Oscillations in GFP concentration as a function of cell cycle phase are weak for the constitutive promoter (red triangles), the *dnaA*P2 promoter (blue circles) and *dnaA*P2-Box2, the promoter not regulated by DnaA (orange triangles). **(B)** The fold-change in volume-specific GFP production rate from *dnaA*P2 shows a clear peak that is not present for a constitutive promoter or the *dnaA*P2-Box2 promoter, which follow similar weak trends. **C** A sinusoidal oscillation for GFP expression from *dnaA*P2 is observed when taking into account the cell cycle phase of lineages with two consecutive generations. **(D,E)** Volume-specific GFP production rate averaged conditionally to time from birth is very similar for the three promoters, while oscillations are enhanced for the *dnaA*P2 promoter when the same data are averaged as a function of the time to division. **(F)** Oscillations in GFP expression from *dnaA*P2 are enhanced when averaged conditionally to time to daughter division. If these oscillations correspond to changes in DnaA activity, they are consistent with the model where DNA replication initiating in the mother cell and terminating in the daughter cell will influence the timing of cell division of the daughter [49]. Error bars (often smaller than symbol size) are standard errors of the mean from a re-sampled distribution obtained by bootstrapping from the experimental data for each bin.

We next set out to ask how the expression of GFP under control of the *dnaA*P2 promoter differs from that of a constitutively expressed gene as a function of the cell cycle. There is only a small reproducible difference in the concentration of GFP as a function of the cell cycle phase when the constitutive and *dnaA*P2 promoters are compared (Fig. 2A). However, the volume-specific GFP production rate from *dnaA*P2 clearly shows an oscillation that is not present in the data for the constitutive P5 promoter or the promoter mutant without DnaA-ATP regulation ("no Act+no Repr", with mutated DnaA Box1 and 2 binding sites in Fig. 1A), which behave similarly in these conditional averages, despite of the repression from SeqA and the different promoter se-

quences (Fig. 2B). Using lineages of two generations we also tested whether these cell cycle phase oscillations are detectable in mother-daughter lineages, which is indeed the case (Fig. 2C).

The near-equivalence of the promoter stripped of DnaA regulation and the constitutive one in Fig. 2BC suggests that the cell cycle dependent SeqA repression alone does not suffice in establishing the reported oscillations, while DnaA-ATP oscillations are essential. The *dnaA*P2 promoter includes a GC-rich discriminator region at the transcription start site which makes it a target for both ppGpp and negative supercoiling dependent regulation [44]. ppGpp levels and negative supercoiling have a strong effect on DNA replication as a function of growth rate [52]. As a control, we measured the expression of GFP from a minimal ribosomal promoter (*rrnB*P1) that also contains a GC-rich discriminator region. Expression of GFP from this promoter does not show a cell cycle dependent oscillation beyond dosage effects (Supplementary Fig. S5), suggesting that ppGpp levels and DNA supercoiling are not sufficient to create a the volume-dependent oscillation.

We can gain more insight on the relationship between these oscillators and the cell cycle by performing averages of the volume-specific production rate that are conditioned on specific cell cycle variables. Specifically, by averaging the data as a function of the time from cell birth, the specific GFP production rate from *dnaA*P2 becomes almost indistinguishable from that of the constitutive promoter (Fig. 2D). However, the amplitude of the oscillation is much greater than that of the constitutive promoter once we average the data as a function of the time to division (Fig. 2E). The two findings suggest that the wild type *dnaA*P2 oscillations are somewhat agnostic of cell birth (or not synchronized with it), and prognostic of (or synchronized with) the next cell division. Fig. 2F shows that the difference between *dnaA*P2 and the constitutive control promoter P5 remains evident when time to daughter's division is used to bin the data. The reason for this is simple if we assume that minima of this oscillator can correspond to the increase in gene copy number and thus initiations of DNA replication. The replication cycle spans two cell cycles under these growth conditions, therefore the time of initiation within the mother cell can have an effect on the time of division of the daughter cell. The results over two-generations lineages also show more clearly how oscillations in volume-specific GFP production rate are symmetric and sinusoidal when under control of the *dnaA*P2 promoter.

Once again, the oscillations are also lost for the construct where both the DnaA binding sites have been mutated ("no Act + no Repr", orange triangles in Fig. 2DEF). However, in the

m3SeqA promoter, when the three downstream SeqA sites are mutated in the context of the wild type *dnaA*P2 sequence, the oscillations do not disappear, but they change in timing and amplitude (Supplementary Fig. S6). This result is in accordance with the idea that SeqA repression of transcription creates a delay in GFP production after the gene has been copied by DNA replication and before its expression is increased by the doubling of gene copy number. Furthermore, this repression contributes to the synchronization of expression of the different copies of the gene reducing the noise of the cell cycle oscillator. The residual oscillation measured by GFP production rate from the m3SeqA promoter should be prominently driven by changes in DnaA activity (note however that in this strain the promoter still contains two SeqA binding sites out of five, which could result in some residual effect of SeqA binding).

These results show that volume-specific GFP production rate from the *dnaA*P2 promoter is a *bona fide* cell cycle oscillator, coupled to the cell division event, and driven by DnaA-ATP levels and SeqA repression. SeqA-dependent repression plays a role in the oscillations but, alone, is insufficient to drive it.

Oscillations in *dnaA*P2 activity are a cell size sensor

The results in Figure 2 show that oscillations emerge when lineages are aligned by cell cycle phase or time to divisions, but not when they are aligned with respect to time from birth. Cell cycle phase aligns the data from individual cells as a function of the the fractional cell cycle progression between the times of cell birth and division and it has been shown to align the time of gene doubling by DNA replication [51]. Given the consensus on the links between cell size and replication initiation, the *dnaA*P2 oscillator can be also expected to follow cell size. Hence, binning the gene expression data as a function of cell volume should result in an improved synchronization of individual cells' oscillations.

We thus proceeded to test the hypothesis that proposes that DnaA activity and/or production rate may be a cell size sensor by binning the data as a function of cell volume instead of cell cycle phase. Fig. 3A shows that volume-binned averages in GFP volume-specific production rate from *dnaA*P2 follow strong oscillations reaching maxima and minima at multiples of a characteristic volume. The same analysis with the data from the constitutive promoter and the mutant *dnaA*P2 promoters also shows oscillations, however of smaller amplitude (Supplementary Fig. S7). The

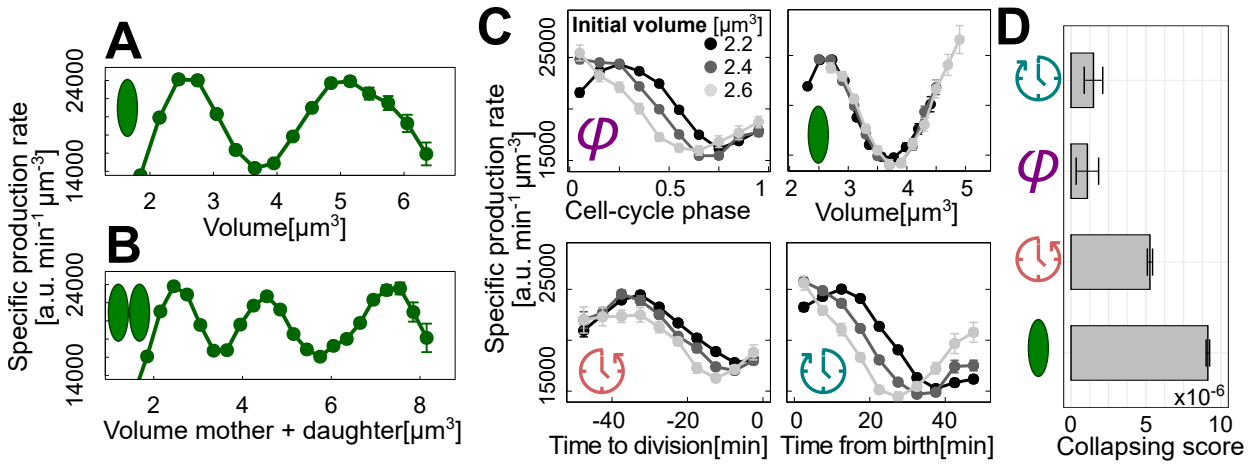

Figure 3: ***dnaA*P2 oscillations sense cell volume** **(A)** Plot of the conditional average of GFP volume-specific production rate from the *dnaA*P2 promoter as a function of cell volume. **(B)** The same average across mother+daughter lineages shows two minima at multiples of a characteristic volume, as expected from replication initiations. **(C)** Volume-specific *dnaA*P2 activity oscillations for cells of different initial size show different degrees of overlap when conditionally averaged as a function of cell cycle phase, time to division, time from birth and cell volume. The differently shaded curves result from data binned according to cell size (volume) at birth ($2.2 \pm 1\mu\text{m}^2$, black , $2.4 \pm 1\mu\text{m}^2$, dark-grey and $2.6 \pm 1\mu\text{m}^2$, light-grey). If the variable in the x axis is the sensed variable, the averages should change independently of the cell size at birth. Data for cell volume shows the best collapse, indicating that the *dnaA*P2 oscillator is a volume sensor. **(D)** Quantification of the collapse of the curves of panel C relative to 11 bins of cell sizes at birth (see Methods). Binning the data by cell size shows the best collapse and binning the data as a function of the time to division shows a good collapse. Error bars are standard errors of the mean obtained by bootstrapping from the experimental data for each bin.

effect of the mutation of the DnaA binding sites shows a significant change in amplitude and phase of the oscillation, consistent with a cell cycle dependent regulation by the concentration of free DnaA-ATP increasing gene expression rate after the increase in gene copy number and decreasing it before (Supplementary Fig. S7). The underlying oscillation of the constitutive and unregulated *dnaA*P2 promoters reflects the doubling of gene dosage upon passage of the replication fork followed by a decrease as cell size further increases. Hence, part of these volume oscillations must be due to indirect dosage effects and dosage-volume correlations, independently from regulation by DnaA or SeqA. Mutation of the SeqA sites shows a visible change in the volume at which oscillation minima occur compared to the wt *dnaA*P2 promoter (Supplementary Fig. S6). This is consistent with repression by SeqA delaying gene expression from the newly replicated promoter.

In order to shed more light into the size-sensing properties of the *dnaA*P2 promoter, we performed joint conditional averages of volume-specific GFP production rate considering different

cell cycle variables (Fig.3B). We performed these averages by further grouping cells based on their size at birth, as we figured that the variables that are more directly coupled to the oscillations should be insensitive to variations of any extrinsic variable. In particular, if the oscillator is a true volume sensor, it should have no memory of size at birth. We divided cells into 11 different birth size classes, and considered binned averages of specific GFP production rate oscillations as a function of cell cycle phase, time to division, time from birth or cell volume. Fig. 3B shows three of the birth size bins relative to an average birth size of $2.2 \pm 0.1\mu\text{m}^3$, $2.4 \pm 0.1\mu\text{m}^3$ and $2.6 \pm 0.1\mu\text{m}^3$. The plots show that volume-binned oscillations are strongly insensitive to birth size, since the data for different birth size bins overlap, while the other variables are sensitive (i.e., the plots relative to different birth size classes do not collapse). Binning by time from birth shows that cells born larger reach the minimum of the oscillation in a shorter time than cells born smaller. Binning by time to division shows the same trend, but results in an intermediate level of collapse. To quantify this behavior, we defined a score of the collapse of different birth-size classes as the inverse of the sum of SE-normalized distances between the oscillations in specific production rate for all 11 birth-size bins (Fig. 3C). The higher the score, the greater the collapse of the oscillations for cells with a different birth size. Fig. 3C shows that cell volume gives the highest score. Time to division gives an intermediate score (still two times higher than those for cell cycle phase and time from birth). Finally, we compared the collapse score using different proxies of cell size (length, surface, volume) as candidates to be sensed by the *dnaA*P2 oscillator, finding that volume is the best candidate [11] (Supplementary Fig. S8).

Volume-sensitive *dnaA*P2 oscillations require the combined activity of DnaA-ATP and SeqA repression.

As noted above, the average specific GFP production rate binned as a function of cell volume for the constitutive promoter, the promoters stripped of DnaA-ATP binding sites and the m3SeqA promoter show oscillations that are lower than the wild-type *dnaA*P2 promoter, but still have an amplitude of 30-40% (Supplementary Fig. S7). Crucially, however, the analysis on the joint conditional averages as a function of birth volume reveals direct volume sensing more effectively (Supplementary Fig. S9).

The comparison of the results of this volume-sensing analysis obtained with the different promoter constructs shows that the collapse score for volume is the highest for the wild-type *dnaA*P2

sequence, remains high for the mutants that are still activated by DnaA and is lost when both DnaA binding sites are mutated (Supplementary Fig. S9). Removing cell cycle dependent repression by mutating the SeqA regulatory sites (m3SeqA reporter mutant) has a small effect on the collapse with volume but loses the collapse with the time to division (Supplementary Fig. S10). In other words, regulation by DnaA-ATP alone is not sufficient to link the oscillation in GFP production rate to the time of cell division, which seems to require repression by SeqA.

The lack of negative regulation by DnaA-ATP reduces the collapse score, but does not abolish it. In this case, repression by SeqA can compensate in part for the lack of DnaA-dependent negative regulation and collapse with time to division is maintained.

Finally, regulation by SeqA alone (in the mutant promoter not regulated by DnaA) is insufficient to couple the oscillations to either volume or cell size at division independently of birth size (Supplementary Fig. S9). Note that the population average gene expression level for this mutant is very similar to that of the wild type (Supplementary Fig. S1) In summary, positive regulation by DnaA is required to maintain gene expression rate as a function of cell volume independently of cell size at birth. An improved level of collapse of the curves is obtained when transcription repression is provided by DnaA-ATP and SeqA.

Together, these data lead us to hypothesize that the *dnaA*P2 oscillator sets its phase according to cell volume through the timing of SeqA regulation and of the increase in gene copy number, which are synchronized with an oscillatory cycle of DnaA activity via DNA-replication dependent regulators such as RIDA, decreasing the DnaA-ATP to DnaA-ADP ratio, at the same time as the transient shut-off of gene expression by SeqA, resulting in a net dilution of DnaA-ATP by cell growth.

At the single cell level, *dnaA*P2 oscillation minima behave as replication initiations

While all the above analyses firmly establish the coupling of the *dnaA*P2 oscillator with cell size and cell division using conditional means, more can be learned considering behavior of single cells [53]. For example, it is important to realize that when using conditional (binned) averages, if some oscillations exist but are not synchronized with respect to the conditioning variable, they cancel out. For example, a flat conditional average results both if the oscillations are not there and

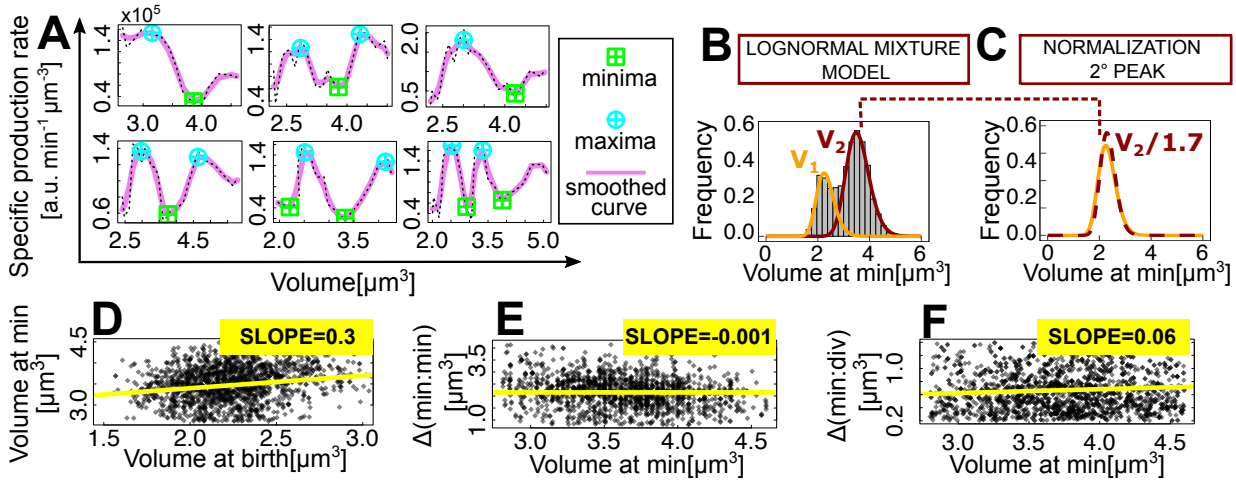

Figure 4: **In single-cells, minima and maxima of *dnaA*P2 oscillations appear at multiples of a characteristic volume and follow the known correlation patterns of initiation of DNA replication. (A)** Oscillations are detectable at the level of single cells. The plots show some single cells *dnaA*P2 tracks *vs* volume (dashed lines), as well as the smoothed tracks (purple solid lines) and the local maxima and minima (symbols) found by our automated algorithm (see Methods). **(B)** The distribution of cell sizes at minima is bimodal with peaks at discrete cell volumes. The bar plots show histograms of cell size at *dnaA*P2 minima, and the solid lines are a fit with a log-normal mixture model, which results in two log-normal distributions. **(C)** If the minima are separated by an adder per origin, the two distributions should collapse if we divide the mean of the second peak by 2. The best collapse is obtained for a factor of 1.7. **(D)** Volume at minima is not constant as a function of volume at birth, i.e. minima are not a sizer. **(E)** Volume added between two consecutive minima is independent on volume at the first minimum (adder between minima). **(F)** Volume added between minima and the next division is independent on volume at the first minimum (adder between minima and division)

when they cancel out. Instead, direct analysis of single cell lineages resolves this ambiguity. In particular, the correlation signatures linking the key events of DNA replication and cell division are well known [15, 18, 19], and our data allows us to ask how single cell *dnaA*P2 oscillations relate to cell cycle progression.

Fig. 4A and Supplementary Fig. S11 show that in our data *dnaA*P2 oscillations are detectable at the level of a single cell track. We defined an automated algorithm that extracts for every cell and lineage the local minima of the *dnaA*P2 oscillations (see Methods). This gives us two key cell cycle events related to *dnaA*P2, plus cell division, for each cell and lineage, where we know instantaneous cell size, growth rate, and interdivision time of each cell. Our data lack a proxy for the initiation of DNA replication, but we can ask whether the *dnaA*P2 oscillations minima in single cells follow similar patterns to the ones recently observed for initiation of DNA replication [15, 19,

20]. We focus in particular on the minima, which could occur downstream of initiation of DNA replication, the moment where SeqA represses transcription and DnaA-ATP is near its highest activity.

In the fast growth condition of our experiments, we found that the distribution of cell sizes at minima is bimodal (Fig. 4B). This is because in some cases, at fast growth, initiation of DNA replication takes place before cell division has occurred, and thus at twice the number of origins and at a cell volume that should be proportional to the number of origins. This is in agreement with the fact that the distribution of cell sizes at initiation of DNA replication in the presence of overlapping rounds of DNA replication should be approximately the sum of two log-normal distributions with means that are one the double of the other [16]. Using a log-normal mixture model to separate the two distributions, we tested whether they would collapse by dividing the mean of the second distribution by two. In our data, the best collapse is achieved by dividing by a factor of 1.7. The small discrepancy could be due to correlations between the volumes at initiation and the probability of extra rounds of replication, previously observed computationally [16]. Additionally, the knowledge of *dnaA*P2 oscillations minima along single-cell lineages allowed us to repeat the analysis reported in Fig. 3 and test for direct sensing of added volume using doubly-conditioned averaged with added volume and volume at birth. Supplementary Fig. S12 shows that the collapse of added volume is as good as for volume itself, hence the analysis does not select which of the two variables is more tightly connected with the oscillator.

Next, we decided to investigate the correlation patterns that link *dnaA*P2 oscillations, DNA replication and cell division. As a control, we verified that our cells show adder correlation patterns between cell birth and division independently of cell size at birth (Supplementary Fig. S13) [54, 55]. To test whether the minima are triggered at a critical size (a ”sizer”) we examined the dependency of the cell size at the minima on birth size (Fig. 4D). The sizer plot is subject to the constraint that initiation size must be larger than birth size; to evaluate correlations between size fluctuations at different cell cycle stages in presence of constraints we used the Bayesian method described in ref. [18]. For a sizer pattern (a circuit that triggers at a critical size) there should be no dependency. Instead, the data clearly show some trend, ruling out this hypothesis. On the other hand, Fig. 4E shows that the added volume between two minima is uncorrelated from cell volume at the first minimum. This recalls the (per origin) inter-initiation adder correlation pattern found by labeling origins or replication fork proteins in single cells [15–17, 19, 20]. Lastly, we considered

the change in cell size between a minimum and cell size of the daughter at division (the analog of the C+D period, if minima are related to initiations). The cell size correlations in this period also follow a near-adder pattern Fig. 4F, as found in the recent literature for the actual C+D period [15, 20].

To summarize, the minima extracted from *dnaA*P2 oscillations in single cells follow the same correlation patterns followed by replication initiation, corroborating our interpretation that the *dnaA*P2 cell cycle oscillator is intimately linked to the single-cell replication cycle. Performing the same analysis on the m3SeqA minima, we find a completely different result (Supplementary Fig. S14). Indeed, single cell m3SeqA oscillation minima show a *sizer* pattern, deviating from replication initiations, and the distribution of cell volumes at m3SeqA minima is peaked at a single volume, which is inconsistent with the expectation from replication initiations. Finally, our slow growth data for *dnaA*P2 oscillation minima (Supplementary Fig. S15), show a more complex pattern, where *dnaA*P2 oscillation minima show adder correlations only above a critical size (of about 2.8 μm^3), and sizer correlations below.

Causal links between cell volume, division and *dnaA*P2 oscillations.

The results so far indicate that the wild type *dnaA*P2 oscillator acts in synchrony with volume and with cell division. However, they are insufficient to establish causal links between these processes. To address this question, we used synchronization and causal analysis of *dnaA*P2 time series along lineages of single cells, as well as perturbation experiments with cell division inhibitor cephalexin. For each lineage, we considered the *dnaA*P2 and m3SeqA cell cycle oscillators, the cell volume time series, and the cell division time series, as three a priori independent signals, to investigate their synchronization and test whether a causality between these signals exists (Fig. 5A and Supplementary Fig. S11). Each of these parameters displays some periodicity throughout several generations.

To test the presence of a time hierarchy connecting specific *dnaA*P2 activity and volume oscillations, we first considered the cross-correlation between these two time series, computed along lineages [56]. Fig. 5B shows that this function is markedly periodic, suggesting a strong coupling, with higher-amplitude peaks for positive time delays. This asymmetry of the cross-correlation function could suggest a ”volume to *dnaA*P2” causality, whereby changes in volume

are prognostic to future changes in *dnaA*P2 oscillations. Importantly, in promoter mutants with mutated DnaA binding sites or in the constitutive promoter the cross-correlations are strongly reduced (Supplementary Fig. S16). Mutation of SeqA binding sites mildly reduces the amplitude of the delayed cross-correlations, but alters the pattern, completely removing the time asymmetry (Supplementary Fig. S16).

Since the results on the m3SeqA promoter lead us to hypothesize that the wild-type *dnaA*P2 oscillator is in synchrony with cell cycle progression through SeqA, hence through sensing of the initiation event by fork transit, we tested the phase locking of the two oscillators as follows [57–59]. We characterized each oscillator with a phase, a linearly increasing variable reset at each cycle, which advances by 1 between successive cycles. Specifically, we defined a *dnaA*P2 phase variable Θ, where $\Theta = 0$ corresponds to the minima of *dnaA*P2 promoter activity and a cell cycle phase Φ as above in this text (Φ = 0 represents birth). These two variables define a periodic square (a torus) $[0, 2\pi)$x$[0, 2\pi)$. Subsequently, as time t increases, the combined phase (Θ,Φ) from each single cell lineage traces a trajectory in this phase space. If their orbits are phase-locked, single lineages follow a diagonal trajectory in this space. Hence, we took a heatmap of the trajectory density from all available data (Supplementary Fig. S17). For the wt *dnaA*P2 oscillator, the phase difference, $\Delta = \Theta - \Phi$ fluctuates around a constant value, hence the heatmap shows two juxtaposed diagonal stripes whose slope is one. Hence the oscillations only depend on the phase difference, as holds for a wide class of synchronized oscillators [60–62]. Conversely the m3SeqA mutant breaks this dependency, as a result of the loss of complete synchrony with the cell cycle phase.

Due to the loss of synchronization with the cell cycle of the m3SeqA oscillator, and due to its loss of delay-time asymmetry in the cross-correlation with volume, we figured that the causal links between the oscillator and the other proxies of the cell cycle may be stronger for the wild-type *dnaA*P2 oscillator. While asymmetric cross-correlations reveal a time hierarchy, one has to be careful when inferring causal relations between two observables because of the existence of a non-zero correlation between two signals does not necessarily imply a causal link [60]. To investigate the directionality of the coupling, we used the Convergent Cross Mapping (CCM) technique, considering *conditional* correlations of one variable with a second one, under the constraint that the former is constrained to its attractor manifold, as reconstructed from the time series using Takens' theorem [63, 64] (see Methods and Supplementary Fig. S18). The output of this analysis, given two time series A and B is a pair of a directional parameters ρ_{AB} and ρ_{BA}, between 0 and

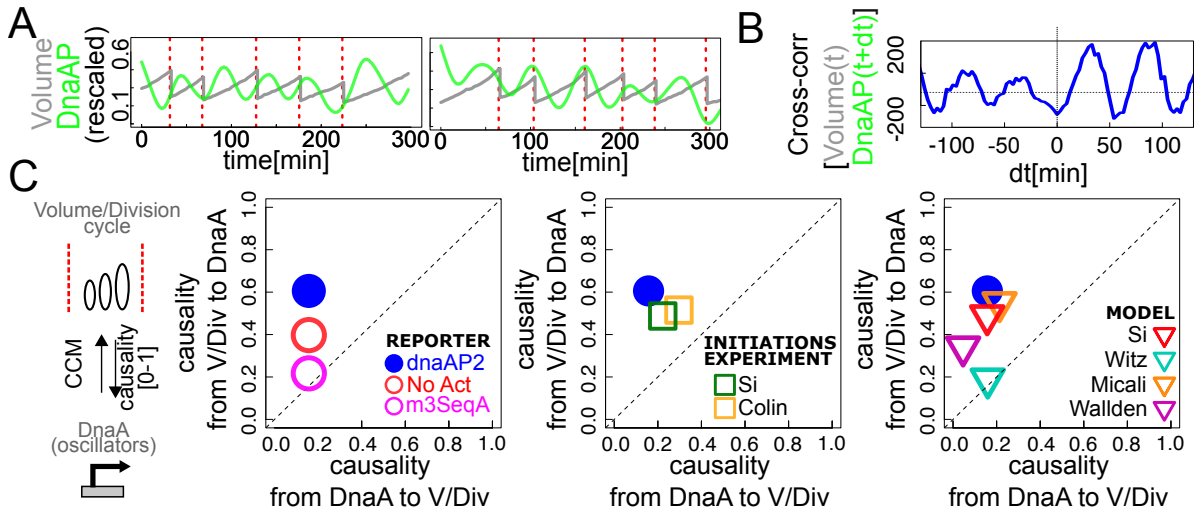

Figure 5: ***dnaA*P2 activity and growth-division are coupled oscillators.** (**A**) Lineages of single cells show a clear oscillation of *dnaA*P2 activity (green), compared here to volume growth (grey) and division events (red), which we considered as three *a priori* independent time series. Volume and *dnaA*P2 activity are normalized here by their average value in order to show them in the same plot. (**B**) Cross-correlation between *dnaA*P2 activity and volume growth is periodic, supporting synchronization between the two oscillators, and asymmetric, supporting a stronger effect of volume changes on future *dnaA*P2 changes than *viceversa*. (**C**) Convergent Cross-Mapping (CCM) identifies causal relationships between oscillators. Left panel: For the wild-type promoter, volume/division are strong causes of *dnaA*P2 changes, but the strength of this causal link decreases in the mutants of the DnaA binding sites and the causality becomes completely symmetric in the mutant of the SeqA binding site. Middle panel: CCM from experimental replication-initiation datasets is consistent with our data for the wild-type promoter. Right panel: CCM from simulated initiation dataset is consistent with our data for the wt *dnaA*P2 promoter for the models from refs. [18, 19].

1, that represent the strength of the causality link from A to B and from B to A. A causal link is witnessed by unequal causality parameters in the two directions $\rho_{AB} \neq \rho_{BA}$.

Fig. 5C summarizes the results of this analysis on our data. In order to try to disentangle the effects of cell volume from cell division events, we first tested the causality between cell volume and an oscillatory signal constructed to have a maximum at division. This analysis returns that volume and cell division are always in a strong symmetric relationship (Supplementary Fig. S19), hence, they are causally indistinguishable. Crucially, Fig. 5C shows instead a strongly asymmetric causality from volume (or division) to dnaAP2. This asymmetric causal link is weakened in the promoter without negative and positive DnaA regulation, and disappears in the m3SeqA promoter, for which the correlation becomes causally symmetric. It is important to point out that these results do not refer to the mutant of the endogenous *dnaA* promoter, but only report how the same endogenous DnaA-ATP oscillations and SeqA transit are read by our reporters when there are

mutations of the binding sites. Hence, the observation that causality is lost when SeqA binding sites (and thus sensing of the passage of the replication fork) are mutated indicates once again that the endogenous *dnaA* promoter as well as our reporter takes relevant input from the fork transit.

Since we have found that *dnaA*P2 oscillatory maxima and minima in single cells follow similar patterns to those found for initiation events, we devised a way to compare the oscillator's causality patterns with those observed for initiations, both in data from refs [19, 20] and in cell-cycle mathematical models proposed in the literature [15, 17–20, 65] (Fig. 5C). To do this, we constructed time series connecting measured or simulated initiation events by sinusoids, in such a way that the minima (or maxima) coincide with initiations in time series taken from data or mathematical models (see Methods). This procedure produces a differentiable oscillatory curve, which can be compared to volume and division time series using convergent cross-mapping. Fig. 5C shows that the predicted causality pattern from experimental data on initiations is completely consistent with the one shown by *dnaA*P2. Fig. 5C shows that only the models from refs [18, 19] are consistent with the causal asymmetry. Both models assume that the pattern between initiations is an adder per origin. The model proposed by Si and coworkers assumes that division is agnostic of the chromosome, and not linked to replication-segregation. The concurrent processes model proposed by Micali and coworkers assumes concurrency of time scales between a cellular process and chromosome replication-segregation setting division through an AND gate.

Going back to our experimental data from wild type *dnaA*P2, our causality analysis using convergent cross mapping shows that cell division or cell size cause *dnaA*P2 oscillations in a much stronger fashion than *dnaA*P2 causes division. This perhaps unintuitive result may have two explanations, (i) there is a strong symmetric coupling between cell division and cell size, and the *dnaA*P2 promoter is a strong size sensor, or (ii) there is a strong symmetric coupling between cell division and cell size, and the *dnaA*P2 promoter is a strong cell division sensor. However, the causal equivalence of cell division and volume in our data do not allow us to distinguish between the two hypotheses. Note that given the essentiality of the SeqA binding sites for the causal asymmetry, it seems reasonable to assume that the crucial sensed event is fork transit, hence (ii) can be restated by saying that replication initiation itself may be a strong sensor of the previous cell division, and (ii) that it may be a strong sensor of cell size.

In order to attempt to resolve this question, we performed additional experiments inhibiting

division by adding cephalexin (Supplementary Fig. S20). Cephalexin-treated cells do not divide, but keep growing and initiating DNA replication, producing an array of nucleoids. Hence, their cell cycle is still somewhat operative. Convergent cross mapping analysis is technically impossible under this perturbation, because the volume time series increases monotonically and lacks an attractor. Interestingly this perturbation does not ablate time-periodic *dnaA*P2 oscillations (Supplementary Fig S20), but conditional averages become flat as soon as the cell sizes exceed the physiological range, suggesting that the synchrony with cell volume is lost [66].

Discussion and Conclusions

An oscillation in DnaA-ATP activity coupled to the cell cycle in *E. coli* is assumed by most, but so far supported only by indirect population-level data [5, 12]. Our data provide a first-time observation of a cell cycle oscillator of gene expression in single *E. coli* cells through the volume-specific production rate of a reporter protein under control of the *dnaA*P2 promoter. This promoter was chosen because it integrates, similarly to the endogenous DnaA production rate, both changes in DnaA activity, via activation and repression by DnaA-ATP, and the timing of initiation of DNA replication via SeqA repression.

The cell cycle dependence of gene expression rate is affected by the doubling of gene copy number after the passage of the replication fork increasing the probability of RNAP binding [51]. We see this as a change in the specific expression rate of a constitutive promoter depending on its genome position (Fig. 2). The volume-specific rate of GFP expression from this promoter decreases until the gene is copied and then it begins to increase again. The volume-specific gene expression rate is therefore not proportional to the increase in cell volume as a function of the cell cycle, similarly to what is observed for the specific growth rate [67, 68].

When we look at the volume-specific production rate from the *dnaA*P2 promoter and its mutants through conditional averages, we see a clear oscillation as a function of cell cycle phase as well as cell volume (Fig. 2 and 3). The oscillations have a considerably larger amplitude than those of the constitutive promoter, showing that the additional regulation of expression by DnaA amplifies the effect of the gene copy number. Furthermore, the oscillations as a function of volume have larger amplitude than those as a function of phase, suggesting a stronger synchronization with respect to the latter variable. The idea that these oscillators may be strong volume (or added vol-

ume) sensors is confirmed by our analyses with doubly-conditional averages (see below). Finally, mutation of the DnaA binding sites alter this oscillation differently depending on whether they decrease repression or both repression and activation by DnaA-ATP, indicating that the concentration of DnaA-ATP (the active form) is not constant as a function of the cell cycle (Supplementary Fig. S7).

The main insights in our study stem from comparing the wt *dnaA*P2 reporter to promoter mutants of the DnaA and SeqA binding sites, allowing us to measure their effect gene expression separately. The data obtained with the promoter with mutations in three SeqA sites (m3SeqA) confirms that regulation by SeqA is not required for relevant cell cycle oscillations. SeqA represses DnaA's gene expression for a window of time (about 10 minutes) after the passage of the replication forks [24]. Accordingly, the comparison with the promoter that lacks the three SeqA sites downstream of the transcription start site (m3SeqA) shows that the oscillations are shifted to smaller volumes or an earlier cell cycle phase (Supplementary Fig. S6). Hence, the activity of these two promoters, m3SeqA and *dnaA*P2, are very different in single cells when averaged conditionally to cell cycle phase or volume: they are shifted, they have different periods and different relationships with time to cell division.

Based on our analyses of conditional averages for the sensing of different variables, both the wt *dnaA*P2 oscillator and the m3SeqA oscillator sense cell volume (Fig. 3 and Supplementary Fig. S10). Interestingly, the m3SeqA promoter, while showing a strong collapse with cell volume, shows poor collapse with time to division. Hence, while the relationship of the oscillator with volume depends on regulation by DnaA, the relationship of the oscillator with time to division appears to rely on the negative regulation by SeqA. This might just point to the relationship between the event of initiation, determining the timing of SeqA repression, and cell division. However, regulation by SeqA alone is not sufficient, as collapse with the time of division is not observed for the promoter without DnaA-ATP regulation (but is still significant for the promoter that is still activated by DnaA). Expression from the promoter that is activated by DnaA-ATP and repressed by SeqA retains a significant level of volume sensing (Supplementary Fig. S9) despite an increased average expression rate (Supplementary Fig. S1). It seems that in these growth conditions timely repression by SeqA is sufficient to maintain some response to volume change. It is interesting to note that, in the context of the native *dnaA* gene, SeqA might also exert some of its cell cycle dependent negative control on gene expression independently of the promoter, via the 15 GATC

sites found at the 3' half of the *dnaA* gene.

Most importantly, the high amplitude of the oscillations in the strains where GFP expression is under control of the promoters regulated by DnaA-ATP allows for an analysis of the minima at the level of single cell lineages. Minima can be thus reliably detected in lineages of the wild type and m3SeqA *dnaA*P2 promoter constructs. In single cells, the minima of the oscillators pinpoint key cell cycle times: for the m3SeqA reporter these are related to the joint contributions of dosage oscillations and DnaA activity-based regulation, and for the wt reporter they are due to SeqA repression as well, and may be expected to co-occur with fork passage a few minutes after replication initiation (the delay should be about eight minutes and the time difference between consecutive frames is three minutes in our experiments). We can obtain significant information about the coupling of gene expression with cell size by studying the behavior of these minima. Minima for the wt *dnaA*P2 oscillator have a striking resemblance with initiations [15, 20], in that they show adder correlations both between subsequent minima and between minima and cell divisions (Fig. 4). Conversely, under regulation by DnaA activity alone (m3SeqA strain), oscillation minima behave as a sizer (Supplementary Fig. S14), the added size between minima depends on the size of the cell at the first minimum, and cell size at these minima shows a lack of correlation with size at birth or division [17]. Equally, when we detect causality between size oscillations and the wt *dnaA*P2 oscillator, we see the same pattern as for a sinusoidal oscillator based on experimental initiation events, robustly across data sets (Fig. 4), and once again this is not the case for the m3SeqA oscillator. Finally, when analyzed as a phase oscillator, only the the wt *dnaA*P2 oscillator shows strong synchronization properties with the cell cycle phase, while the m3SeqA oscillator shows a more irregular synchronization behavior (Fig. S17).

Hence, it appears from our data that the combination of DnaA activity and dosage proxied by the m3SeqA oscillator does not encode initiations, but the *dnaA*P2 oscillator may do, and the additional SeqA repression is crucial for this.

Finally, at slow growth, we see an intriguingly complex pattern for the minima of the wt *dnaA*P2 oscillator (Supplementary Fig. S15). Only oscillator minima in larger-than-average cells show the adder correlations that are observed for initiations. Smaller-than-average cells, instead, show a sizer pattern, similar to that observed for the m3SeqA oscillator minima at fast growth. We hypothesize that, due to the low effect of SeqA repression at slow growth visible in our ex-

periments (Supplementary Fig. S1) and compatible with classic observations [24, 26, 46], the wt *dnaA*P2 oscillator is mostly dependent on DnaA activity and is therefore less coupled to initiations at smaller cell sizes.

Currently, theoretical predictions are based on rather complex parameter-rich models built on population-average measurements [23, 69, 70]. The most recent model [23] proposes that robust replication control is a result of initiation at a critical threshold number of DnaA-ATP proteins whose concentration oscillates with the cell cycle, and that this circuit is a sizer, based on sensing the origin density. This study proposes that the DnaA-ATP sizer would not be observable, due to fluctuations in the density threshold for replication initiation (which give rise to the observed inter-initiation adder patterns in their model). Via the activity of the DnaA-regulated promoter, here we can observe a sizer in the oscillation of volume-specific GFP expression rate in the m3SeqA mutant, which depends on the oscillation in the concentration of free DnaA-ATP, not its amount.

While our data for the m3SeqA promoter do not allow to clearly separate the effects of DnaA activity from gene dosage, the comparison with the constitutive promoter and the mutated *dnaA* promoters is consistent with repression taking place mainly before the increase in gene copy number and activation taking place after SeqA has dissociated. This could reflect a rapid decrease in DnaA-ATP concentration due to the combined effects of RIDA, SeqA repression of DnaA expression and dilution due to cell growth. In the absence of SeqA repression of the reporter construct, the sizer-like m3SeqA oscillator minima would then correspond to DnaA activity peaks. Our data could thus be consistent with a scenario where the amount of DnaA-ATP must reach a threshold level for OriC activation, which is followed by DnaA inactivation. The adder pattern of initiations is consistent with the idea that additional factors play an important role in the changes in DNA conformation required for the robust regulation of the timing of assembly of the replication forks, whose result is observed in the wt *dnaA*p2 promoter oscillator [2, 71–73].

In summary, here we show that in single cells, for all the promoters studied here, the volume-specific gene expression rate follows a basal cell-cycle oscillation independently of specific promoter regulation, because of gene dosage changes. In the case of *dnaA*P2, a coherent interpretation of our data is that regulation by DnaA-ATP enhances the oscillation relative to the promoter where the DnaA binding sites have been mutated (whose oscillation is indistinguishable from the basal one), and renders it responsive to cell volume changes via activation and repression at different

times of the cell cycle. Prevention of transcription initiation by SeqA decreases the production rate post-initiation, delays the increase in gene expression due to the doubling in gene dosage, and synchronizes the oscillations with the initiation of DNA replication, establishing a causal link of gene expression with cell division. A recent study by Knoppel and coworkers [74] has analyzed initiation patterns of many mutants of regulators of DnaA activity. Its main conclusion is that many circuit elements that are generally considered important for faithful initiation, including cell cycle specific regulation of DnaA expression, DARS sites, *datA*, and acidic phospholipids, are non-essential, while the core element of the circuit for triggering initiation in a timely manner appears to be the regulation of the ATP- vs ADP-bound fractions of DnaA by the RIDA process associated with fork progression. On the other hand, another recent study by Boesen and coworkers[36] shows that the DNA replication cycle is very similar to the wild type strain when RIDA and the other DnaA activity regulators, *datA* and the DARS sites, are inactive, showing that the inherent ATP hydrolysis activity of DnaA can be sufficient to drive a stable replication cycle. Further work will be required to determine how the activity of these different regulatory factors maintains a robust replication program in the presence of perturbations such as growth shifts or DNA damage [75, 76]. To elucidate more directly these hypotheses, the approach used here can be used to measure the effect on the oscillations of DnaA activity of endogenous perturbations of regulators of DnaA-ATP of DnaA-ADP ratio.

Together, our data shed new light on the complex homeostatic control of initiation of DNA replication via the regulation of gene expression.

METHODS

Strains and growth medium. The experiments were carried out with the wild-type *E. coli* strain BW25113, the parent strain of the Keio collection [77], which has been fully sequenced [78]. Promoter reporter constructs were inserted in the chromosome close to the origin of replication at ori3 (4413507 bp, nearest gene aidB). Promoters express gfpmut2, a fast folding fluorescent protein. A kanamycin resistance cassette (KanR) is divergently expressed from each promoter-gfpmut2 cassette. This protein exhibits bright green fluorescence when exposed to light in the blue to ultraviolet range, so was used as biological marker. The fluorescent strains absorb light at one wavelength (≈ 395 nm), then emit it at another (≈ 509 nm). Then filters transmit only the emitted light. The native dnaA promoter region (dnaAP) contains two promoter sequences, dnaAP1 and dnaAP2. While dnaAP1 provides a basal level of expression, dnaAP2 contains all of the sequence elements usually found in stable RNA promoters. Several DnaA-binding sites are found both upstream and overlapping the main promoter elements, resulting in negative autoregulation of transcription by DnaA–ATP. Our DnaA reporter is identical to the native one but lacks the dnaAP1. Our constitutive reporter P5 is based on a strong exogenous promoter with consensus -10 and -35 sequences lacking any transcription factor regulation, as well as lacking a GC-rich ppGpp discriminator region at the transcription initiation site that would make it sensitive to inhibition by ppGpp. Our ribosomal reporter "P1" is derived from the P1 promoter of the ribosomal RNA operon rrnB and therefore contains a GC-rich discriminator region at the transcription start site. The upstream end of the promoter has been omitted, thus deleting the binding sites for any transcriptional regulators Ribosomal and constitutive promoters are also inserted in the chromosome close to the replication terminus at ter3 (1395706 bp, nearest gene ydaA). Bacteria were grown overnight in M9+0.4% glucose at 30°C. Overnight cultures were diluted 500:1 in new growth medium and returned to the incubator for 3-4 h. This is important to guarantee bacteria to be in their exponential phase when injected into the device. Experiments were carried out at 30°C in two growth conditions: a "slow" growth condition in M9-glucose with an average doubling time of 75 ± 5min and in a "fast" growth medium, M9-glucose-casamino acids, with an average doubling time of 45 ± 5min. We verified that the different levels of expression of the GFP gene in the different strains do not have an effect on cell growth. Doubling time and cell size are consistent between all the mutants (Supplementary Fig. S21).

Mother machine experiments. We used a microfluidic ”mother machine” device that with two large feeding channels. The bacteria are trapped in the microfluidic channel thanks to their narrower shape on one side. PDMS (Polydimethylsiloxane) devices from the mould were obtained by standard procedure with plasma cleaner. Before loading bacteria into the device, each chip was treated with a solution of bovine serum albumin (BSA) to minimize bacterial interactions and binding to the glass or PDMS components. Devices were pipetted with 5 μL of 2% BSA and incubated at 30°C for 1 h. Passivated chips were rinsed with fresh filtered medium. After that 1ml of culture was injected manually. Both feeding channels are coupled with a flow sensor. Using its feedback loop, we can monitor and control flow rate in our microfluidic setup while keeping stability and responsiveness of pressure driven flows. This technology enables us to set up robust and long term microfluidic experiments. A home-built temperature control system is used to maintain the entire setup at 30°C. We use Nikon Inverted Microscope ECLIPSE Ti-E with 100X oil objective high NA (Numerical Aperture) lens, coupled with a Nikon Perfect Focus System (PFS) to rectify drift in focus due to emitted fluorescence light from the excitation light for observation with a CCD camera. A xy motion plate is used to memorize and loop over different ROIs (Region Of Interests) at specified interval of time. In order to have the same set of channels for a given field of view and to not have any loss of focus during the experiment we built a support for the device with a 3D printer. This avoids also minimal displacements of the device. In this experimental setup, fluorescence images are taken with light from a blue LED passed through a GFP filter. Different strains of bacteria may express gfp at different levels. Henceforth it becomes necessary to adjust the exposure time and acquisition parameters for different strains in-order to obtain enough fluorescence and simultaneously not saturate the pixels. Moreover it is very important not to expose the bacteria to this light during the first few hours when the bacteria is adapting to the microfluidic device.

Data analysis pipeline. The camera captured 16 bit images at 512 x 512 pixel resolution with the length of one pixel equal to 0.1067μm. The motorized stage and camera were programmed to cycle between at most 40 fields of view, each spanning roughly 8 microchannels, every 3 min. Final movies are of .nd2 format and are first analysed with Fiji software. Background subtraction is performed using a 50 pixel rolling ball technique, and different positions are stored separately as a set of .tiff image files. Channels with a good number of bacteria are selected manually and stored in different folders. For segmentation and tracking, we started from codes developed by

Mia Panlilio (Cambridge University) and we added necessary modifications to optimize it for our experimental setup. Before starting, we select the time window where bacteria are in steady state in a given growth medium. To correct segmentation and tracking errors we applied a set of filters. First, we consider cells with an entire life cycle tracked i.e. both parent and daughter(s) were at least partially tracked. Second, division event has to be symmetric, i.e. each daughter has a volume between 0.4 and 0.6 of the one of the mother. This step aims to eliminate filamentous cells and segmentation artefacts. Third, doubling time is greater than 15 mins (pysiological lower limit is 15-20 min). Last, initial/final volume, initial/final width and initial/final growth rate are inside the 95% confidence interval. Before computing the discrete derivative of fluorescence and area (as central derivatives defined across three subsequent frames) we removed outliers from fluorescence and area traces and we substituted them by linear interpolation. Custom R notebooks were written to handle and analyse these large, non-uniform datasets. All datasets were grouped based on strain and growth medium in different R object. An exploratory data analysis is necessary to check if datasets are consistent and filters worked well. Custom functions were written to compute the discrete derivatives and the different normalizations.

Volume and gene dosage estimation. We calculate the volume describing a cell as a cylinder with two hemispherical caps,

$$V(t) = \pi(l(t) - w)\left(\frac{w}{2}\right)^2 + \frac{4}{3}\pi\left(\frac{w}{2}\right)^3 , \tag{1}$$

where w was taken as a cell-cycle average of the average measured cell width. The expected gene copy number was computed from the Cooper-Helmstetter model [79]. Replication of the *E. coli* chromosome begins from a single origin and oppositely oriented replication forks proceed symmetrically along the genome to complete replication. Since on average a cell divides at a time $C + D$ (≈ 60 min) after replication initiation, an average time lag B before initiation is necessary to make the total replication time $B + C + D$ an integer multiple of the doubling time τ. Thus, defining $n = \mathrm{Int}(C + D/\tau)$ as the integer number of times that τ divides $C + D$, one has that $B+C+D = (n+1)\tau$. More generally, we can consider a gene at a chromosomal position defined by its normalized distance from Ori, i.e. $l = 0$ represents a gene in Ori and $l = 1$ a gene in Ter.

The copy number of this gene, g , changes during the cell cycle following

$$g(t) := \begin{cases} 2^{n'} & \text{if } 0 < t < (n'+1)\tau - (c(1-l)+D) \\ 2^{n'+1} & \text{if } (n'+1)\tau - (c(1-l)+D) < t < \tau \end{cases} , \tag{2}$$

where $n' = \text{Int}\left[\frac{C(1-l)+D}{\tau}\right]$. By averaging over the cell cycle one gets the expected gene

$$g = \langle g(t) \rangle_{\text{cell cycle}} = \frac{1}{\tau}\int_0^\tau g(t)dt = 2^n\{1 - n + \mu[C(1-l)+D]\} . \tag{3}$$

Convergent cross mapping. Convergent Cross Mapping (CCM) is a method for causality inference based on Takens' theorem [63] and developed in ref. [64]. Takens' theorem shows that time-delay embedding of a one-dimensional time series provides a 1–1 mapping of system dynamics from the original phase space (constructed with all system variables) to the reconstructed shadow phase space, as long as the latter has sufficient dimensions to contain the original attractor. Supplementary Figure S18 summarizes the main steps of the CCM method. Shortly, it reconstructs a shadow attractor from one time series at a time and uses these coordinates to compute conditional correlations at fixed values of the shadow attractor of the variable. Since they are based on different constraints, the conditional correlations are not symmetric, and reveal causal links. We used the R package multispatialCCM to implement CCM (`https://CRAN.R-project.org/package=multispatialCCM`). CCM was used on our experimental data on volume, divisions, and dnaAP2 oscillation time series, on DNA replication initiation data from the literature and on simulated data. In our data, we used volume and dnaAP oscillator time series, and a cell division time series was defined as a continuous process with narrow peaks around each experimental division event. For initiation of DNA replication data, we used two datasets from the literature where initiation of DNA replication and cell division were tracked within the cell cycle [19, 20], and we defined a putative dnaAP oscillator time series by assuming a sinusoid between 0 and 1 with the minima at consecutive initiations (Supplementary Fig. S18B). We also simulated four different models described in the literature: a model where replication initiation sets cell division through a timer, from ref. [65]; a model where DNA replication initiation set cell division through an adder [15]; a model where replication and an inter-division concurrently limit cell division [17, 18]; and a model where DNA replication has no direct influence on the timing of division [19]. The codes and parameter values are those used in ref. [20].

References

1. Ohbayashi, R. *et al.* Evolutionary Changes in DnaA-Dependent Chromosomal Replication in Cyanobacteria. *Frontiers in Microbiology* **11** (2020).
2. Leonard, A. C., Rao, P., Kadam, R. P. & Grimwade, J. E. Changing Perspectives on the Role of DnaA-ATP in Orisome Function and Timing Regulation. *Frontiers in Microbiology* **10,** 2009 (2019).
3. Erzberger, J. & Berger, J. Evolutionary relationships and structural mechanisms of AAA+ proteins. *Annual review of biophysics and biomolecular structure* **35,** 93–114 (2006).
4. Duderstadt, K. E. *et al.* Origin Remodeling and Opening in Bacteria Rely on Distinct Assembly States of the DnaA Initiator. *The Journal of Biological Chemistry* **285,** 28229–28239 (2010).
5. Kurokawa, K., Nishida, S., Emoto, A., Sekimizu, K. & Katayama, T. Replication cycle-coordinated change of the adenine nucleotide-bound forms of DnaA protein in Escherichia coli. *The EMBO Journal* **18,** 6642–6652 (1999).
6. Katayama, T., Kasho, K. & Kawakami, H. The DnaA Cycle in Escherichia coli: Activation, Function and Inactivation of the Initiator Protein. *Frontiers in Microbiology* **8** (2017).
7. Hill, N. S., Kadoya, R., Chattoraj, D. K. & Levin, P. A. Cell size and the initiation of DNA replication in bacteria. *PLoS genetics* **8,** e1002549 (2012).
8. Si, F. *et al.* Invariance of Initiation Mass and Predictability of Cell Size in Escherichia coli. *Current biology: CB* **27,** 1278–1287 (2017).
9. Donachie, W. D. Relationship between Cell Size and Time of Initiation of DNA Replication. *Nature* **219,** 1077–1079 (1968).
10. Zheng, H. *et al.* General quantitative relations linking cell growth and the cell cycle in Escherichia coli. *Nature Microbiology* (2020).
11. Zheng, H. *et al.* Interrogating the Escherichia coli cell cycle by cell dimension perturbations. *Proceedings of the National Academy of Sciences* **113,** 15000–15005 (2016).
12. Donachie, W. D. & Blakely, G. W. Coupling the initiation of chromosome replication to cell size in Escherichia coli. *Current Opinion in Microbiology* **6,** 146–150 (2003).

13. Løbner-Olesen, A., Skarstad, K., Hansen, F. G., von Meyenburg, K. & Boye, E. The DnaA protein determines the initiation mass of Escherichia coli K-12. *Cell* **57,** 881–889 (1989).

14. Wold, S., Skarstad, K., Steen, H. B., Stokke, T. & Boye, E. The initiation mass for DNA replication in Escherichia coli K-12 is dependent on growth rate. *The EMBO Journal* **13,** 2097–2102 (1994).

15. Witz, G., van Nimwegen, E. & Julou, T. Initiation of chromosome replication controls both division and replication cycles in E. coli through a double-adder mechanism. *eLife* **8** (2019).

16. Ho, P.-Y. & Amir, A. Simultaneous regulation of cell size and chromosome replication in bacteria. *Frontiers in Microbiology* **6** (2015).

17. Micali, G., Grilli, J., Marchi, J., Osella, M. & Cosentino Lagomarsino, M. Dissecting the Control Mechanisms for DNA Replication and Cell Division in E. coli. *Cell Reports* **25,** 761–771.e4 (2018).

18. Micali, G., Grilli, J., Osella, M. & Lagomarsino, M. C. Concurrent processes set E. coli cell division. *Science Advances* **4,** eaau3324 (2018).

19. Si, F. *et al.* Mechanistic Origin of Cell-Size Control and Homeostasis in Bacteria. *Current Biology* **29,** 1760–1770.e7 (2019).

20. Colin, A., Micali, G., Faure, L., Lagomarsino, M. & van Teeffelen, S. Two different cell-cycle processes determine the timing of cell division in Escherichia coli. *eLife* **10** (2021).

21. Tiruvadi-Krishnan, S. *et al.* Replication-related control over cell division in Escherichia coli is growth-rate dependent (2021).

22. Harris, L. K. & Theriot, J. A. Relative Rates of Surface and Volume Synthesis Set Bacterial Cell Size. *Cell* **165,** 1479–1492 (2016).

23. Berger, M. & Wolde, P. R. T. Robust replication initiation from coupled homeostatic mechanisms. *Nature communications* **13,** 6556 (2022).

24. Campbell, J. L. & Kleckner, N. E. coli oriC and the dnaA gene promoter are sequestered from dam methyltransferase following the passage of the chromosomal replication fork. *Cell* **62,** 967–979 (1990).

25. Riber, L. & Løbner-Olesen, A. Coordinated replication and sequestration of oriC and dnaA are required for maintaining controlled once-per-cell-cycle initiation in Escherichia coli. *Journal of Bacteriology* **187,** 5605–5613 (2005).

26. Lu, M., Campbell, J. L., Boye, E. & Kleckner, N. SeqA: a negative modulator of replication initiation in E. coli. *Cell* **77,** 413–426 (1994).

27. Atlung, T., Clausen, E. S. & Hansen, F. G. Autoregulation of the dnaA gene of Escherichia coli K12. *Molecular & general genetics: MGG* **200,** 442–450 (1985).

28. Speck, C., Weigel, C. & Messer, W. ATP- and ADP-dnaA protein, a molecular switch in gene regulation. *The EMBO journal* **18,** 6169–6176 (1999).

29. Saggioro, C., Olliver, A. & Sclavi, B. Temperature-dependence of the DnaA–DNA interaction and its effect on the autoregulation of dnaA expression. *Biochemical Journal* **449,** 333–341 (2013).

30. Kato, J.-i. & Katayama, T. Hda, a novel DnaA-related protein, regulates the replication cycle in Escherichia coli. *The EMBO Journal* **20,** 4253–4262 (2001).

31. Kasho, K. & Katayama, T. DnaA binding locus datA promotes DnaA-ATP hydrolysis to enable cell cycle-coordinated replication initiation. *Proceedings of the National Academy of Sciences of the United States of America* **110,** 936–941 (2013).

32. Skarstad, K. & Katayama, T. Regulating DNA replication in bacteria. *Cold Spring Harbor Perspectives in Biology* **5,** a012922 (2013).

33. Fujimitsu, K., Senriuchi, T. & Katayama, T. Specific genomic sequences of E. coli promote replicational initiation by directly reactivating ADP-DnaA. *Genes & Development* **23,** 1221–1233 (2009).

34. Frimodt-Møller, J., Charbon, G., Krogfelt, K. A. & Løbner-Olesen, A. DNA Replication Control Is Linked to Genomic Positioning of Control Regions in Escherichia coli. *PLOS Genetics* **12,** e1006286 (2016).

35. Miyoshi, K., Tatsumoto, Y., Ozaki, S. & Katayama, T. Negative feedback for DARS2-Fis complex by ATP-DnaA supports the cell cycle-coordinated regulation for chromosome replication. *Nucleic acids research* **49,** 12820–12835 (22 2021).

36. Boesen, T. *et al.* Robust control of replication initiation in the absence of DnaA-ATP DnaA-ADP regulatory elements in Escherichia coli (2022).

37. Espeli, O., Mercier, R. & Boccard, F. DNA dynamics vary according to macrodomain topography in the E. coli chromosome. *Molecular Microbiology* **68,** 1418–1427 (2008).

38. Long, Z. *et al.* Measuring bacterial adaptation dynamics at the single-cell level using a microfluidic chemostat and time-lapse fluorescence microscopy. *The Analyst* **139,** 5254–5262 (2014).

39. Messer, W. & Weigel, C. DnaA as a transcription regulator. *Methods Enzymol.* **370,** 338–349 (2003).

40. Menikpurage, I. P., Woo, K. & Mera, P. E. Transcriptional Activity of the Bacterial Replication Initiator DnaA. *Frontiers in Microbiology* **12,** 662317 (2021).

41. Cormack, B. P., Valdivia, R. H. & Falkow, S. FACS-optimized mutants of the green fluorescent protein (GFP). *Gene* **173,** 33–38 (1996).

42. Hansen, E. B., Hansen, F. G. & von Meyenburg, K. The nucleotide sequence of the dnaA gene and the first part of the dnaN gene of Escherichia coli K-12. *Nucleic Acids Research* **10,** 7373–7385 (1982).

43. Travers, A. & Muskhelishvili, G. DNA supercoiling - a global transcriptional regulator for enterobacterial growth? *Nature Reviews. Microbiology* **3,** 157–169 (2005).

44. Chiaramello, A. E. & Zyskind, J. W. Expression of Escherichia coli dnaA and mioC genes as a function of growth rate. *Journal of Bacteriology* **171,** 4272–4280 (1989).

45. Messer, W. & Weigel, C. DnaA initiator—also a transcription factor. *Molecular Microbiology* **24,** 1–6 (1997).

46. Wilkinson, T. G. *et al.* The Synchrony Phenotype Persists after Elimination of Multiple GATC Sites from the dnaA Promoter of Escherichia coli. *Journal of Bacteriology* **188,** 4573–4576 (2006).

47. Kedar, G. C. *et al.* Role of DNA methylation at GATC sites in the dnaA promoter, dnaAp2. *Journal of Molecular Microbiology and Biotechnology* **2,** 301–310 (2000).

48. Panlilio, M. *et al.* Threshold accumulation of a constitutive protein explains E. coli cell-division behavior in nutrient upshifts. *Proceedings of the National Academy of Sciences* **118** (2021).

49. Cooper, S. & Helmstetter, C. E. Chromosome replication and the division cycle of Escherichia coli B/r. *Journal of Molecular Biology* **31,** 519–540 (1968).

50. Brenner, N. *et al.* Universal protein distributions in a model of cell growth and division. *Physical review. E, Statistical, nonlinear, and soft matter physics* **92,** 042713 (4 2015).

51. Walker, N., Nghe, P. & Tans, S. J. Generation and filtering of gene expression noise by the bacterial cell cycle. *BMC Biology* **14,** 11 (2016).

52. Fernández-Coll, L. *et al.* The Absence of (p)ppGpp Renders Initiation of Escherichia coli Chromosomal DNA Synthesis Independent of Growth Rates. *mBio* **11** (2020).

53. Osella, M., Tans, S. J. & Cosentino Lagomarsino, M. Step by Step, Cell by Cell: Quantification of the Bacterial Cell Cycle. *Trends in Microbiology* **25,** 250–256 (2017).

54. Campos, M. *et al.* A Constant Size Extension Drives Bacterial Cell Size Homeostasis. *Cell* **159,** 1433–1446 (2014).

55. Taheri-Araghi, S., Brown, S. D., Sauls, J. T., McIntosh, D. B. & Jun, S. Single-Cell Physiology. *Annual Review of Biophysics* **44,** 123–142 (2015).

56. Kiviet, D. J. *et al.* Stochasticity of metabolism and growth at the single-cell level. *Nature* **514,** 376–379 (2014).

57. Droin, C., Paquet, E. R. & Naef, F. Low-dimensional dynamics of two coupled biological oscillators. *Nature Physics* **15,** 1086–1094 (2019).

58. Feillet, C. *et al.* Phase locking and multiple oscillating attractors for the coupled mammalian clock and cell cycle. *Proceedings of the National Academy of Sciences* **111,** 9828–9833 (2014).

59. Bieler, J. *et al.* Robust synchronization of coupled circadian and cell cycle oscillators in single mammalian cells. *Molecular Systems Biology* **10,** 739 (2014).

60. Pikovsky, A., Rosenblum, M. & Kurths, J. Synchronization: A universal concept in nonlinear sciences, 433.

61. Goldstein, R. E., Polin, M. & Tuval, I. Noise and Synchronization in Pairs of Beating Eukaryotic Flagella. *Physical Review Letters* **103,** 168103 (2009).

62. Kotar, J., Leoni, M., Bassetti, B., Lagomarsino, M. C. & Cicuta, P. Hydrodynamic synchronization of colloidal oscillators. *Proceedings of the National Academy of Sciences* **107,** 7669–7673 (2010).

63. Takens, F. *Detecting strange attractors in turbulence* in *Dynamical Systems and Turbulence, Warwick 1980* (eds Rand, D. & Young, L.-S.) (Springer, Berlin, Heidelberg, 1981), 366–381.

64. Sugihara, G. *et al.* Detecting Causality in Complex Ecosystems. *Science* **338,** 496–500 (2012).

65. Wallden, M., Fange, D., Lundius, E. G., Baltekin, Ö. & Elf, J. The Synchronization of Replication and Division Cycles in Individual E. coli Cells. *Cell* **166,** 729–739 (2016).

66. Sánchez-Gorostiaga, A. *et al.* Life without Division: Physiology of Escherichia coli FtsZ-Deprived Filaments. *mBio* **7,** e01620–16 (2016).

67. Nordholt, N., van Heerden, J., Kort, R. & Bruggeman, F. J. Effects of growth rate and promoter activity on single-cell protein expression. *Scientific Reports* **7,** 6299 (2017).

68. Kar, P., Tiruvadi-Krishnan, S., Männik, J., Männik, J. & Amir, A. *To bin or not to bin: analyzing single-cell growth data* preprint (Microbiology, 2021).

69. Grant, M. A. *et al.* DnaA and the timing of chromosome replication in Es-cherichia coli as a function of growth rate. *BMC Systems Biology* **5,** 201 (2011).

70. Zhang, Q., Zhang, Z. & Shi, H. Cell Size Is Coordinated with Cell Cycle by Regulating Initiator Protein DnaA in E. coli. *Biophysical Journal* **119,** 2537–2557 (2020).

71. Kleckner, N. E., Chatzi, K., White, M. A., Fisher, J. K. & Stouf, M. Coordination of Growth, Chromosome Replication/Segregation, and Cell Division in E. coli. *Frontiers in Microbiology* **9,** 1469 (2018).

72. Zaritsky, A. & Woldringh, C. L. Chromosome replication, cell growth, division and shape: a personal perspective. *Frontiers in Microbiology* **6** (2015).

73. Magnan, D. & Bates, D. Regulation of DNA Replication Initiation by Chromosome Structure. *Journal of Bacteriology* **197** (ed Margolin, W.) 3370–3377 (2015).

74. Knöppel, A., Broström, O., Gras, K., Fange, D. & Elf, J. The coordination of replication initiation with growth rate in Escherichia coli. *bioRxiv* (2022).

75. Sutera, V. A. & Lovett, S. T. The role of replication initiation control in promoting survival of replication fork damage. *Molecular Microbiology* **60,** 229–239 (2006).

76. Quiñones, A., Jueterbock, W. R. & Messer, W. DNA lesions that block DNA replication are responsible for the dnaA induction caused by DNA damage. *Molecular & general genetics: MGG* **231,** 81–87 (1991).

77. Baba, T. *et al.* Construction of Escherichia coli K-12 in-frame, single-gene knockout mutants: the Keio collection. *Molecular Systems Biology* **2,** 2006.0008 (2006).

78. Grenier, F., Matteau, D., Baby, V. & Rodrigue, S. Complete Genome Sequence of Escherichia coli BW25113. *Genome Announcements* **2** (2014).

79. Cooper, S. Cell division and DNA replication following a shift to a richer medium. *Journal of Molecular Biology* **43,** 1–11 (1969).

Acknowledgements We are grateful to Nancy Kleckner for useful feedback on our work, and to Petra Levin, Johan Elf and Philippe Nghe for useful discussions.

Competing Interests The authors declare that they have no competing financial interests.

Correspondence Correspondence and requests for materials should be addressed to MCL (email:marco.cosentino-lagomarsino@ifom.eu) and BS (email:bianca.sclavi@sorbonne-universite.fr).